6-25-2001

Dislocation-Controlled Perforated Layer Phase in a Peo-B-Ps Diblock Copolymer

Lei Zhu
University of Akron Main Campus

Ping Huang
University of Akron Main Campus

Stephen Z. D. Cheng
University of Akron Main Campus, scheng@uakron.edu

Qing Ge
University of Akron Main Campus

Roderic P. Quirk
University of Akron Main Campus

See next page for additional authors

Authors

Lei Zhu, Ping Huang, Stephen Z. D. Cheng, Qing Ge, Roderic P. Quirk, Edwin L. Thomas, Bernard Lotz, Jean-Claude Wittmann, Benjamin S. Hsiao, Fengji Yeh, and Lizhi Liu

Dislocation-Controlled Perforated Layer Phase in a PEO-*b*-PS Diblock Copolymer

Lei Zhu,[1] Ping Huang,[1] Stephen Z. D. Cheng,[1,*] Qing Ge,[1] Roderic P. Quirk,[1] Edwin L. Thomas,[2] Bernard Lotz,[3]
Jean-Claude Wittmann,[3] Benjamin S. Hsiao,[4] Fengji Yeh,[4] and Lizhi Liu[4]

[1]*Maurice Morton Institute and Department of Polymer Science, The University of Akron, Akron, Ohio 44325-3909*
[2]*Department of Materials Science and Engineering, Massachusetts Institute of Technology, Cambridge, Massachusetts 02139*
[3]*Institute Charles Sadron, 6 Rue Boussingault, Strasbourg 67083, France*
[4]*Department of Chemistry, The State University of New York at Stony Brook, Stony Brook, New York 11794-3400*
(Received 8 March 2001)

Small angle x-ray analyses show that the shear-induced hexagonal perforated layer phase in a poly(ethylene oxide)-*b*-polystyrene diblock copolymer consists of trigonal ($R\bar{3}m$) twins and a hexagonal ($P6_3/mmc$) structure, with trigonal twins being majority components. Transmission electron microscopy reveals that the hexagonal structure is generated through sequential intrinsic stacking faults on the second layer from a previous edge dislocation line, while the trigonal twins are formed by successive intrinsic stacking faults on neighboring layers due to the plastic deformation under mechanical shear.

Diblock copolymers are of tremendous scientific interest due to their ability to self-assemble into various ordered morphologies on a nanometer length scale [1]. Besides three conventional phase morphologies for diblock copolymers, i.e., lamellae, hexagonal cylinders, and body-centered cubic spheres, additional complex morphologies have also been observed such as double gyroid [2,3] and hexagonal perforated layers (HPL) [4–11]. The stacking sequences of the hexagonal perforations in the HPL phase have been modeled as *ABCABC* (trigonal $R\bar{3}m$) and/or *ABAB* arrangements (hexagonal $P6_3/mmc$). Theoretical calculations [12–14] were also carried out using a broad base of symmetries (e.g., fcc, hcp, $R\bar{3}m$, $P6_3/mmc$, and bcc, etc.) to predict the stability of the shear-induced HPL phase. Experimental findings suggested that the HPL phase was induced by mechanical shear, and it was a nonequilibrium, long-lived metastable phase or intermediate state [10,11,15].

In order to determine the phase structure of the shear-induced HPL phase and further investigate the origin of this unique phase, we study a poly(ethylene oxide)-*b*-polystyrene (PEO-*b*-PS) diblock copolymer with $M_n^{\text{PEO}} = 11$ kg/mol and $M_n^{\text{PS}} = 17$ kg/mol. A detailed method of the sequential anionic block copolymerization for this sample can be obtained from Ref. [16]. The PEO-block volume fraction is 0.39. The sample was cast from toluene and annealed at 100 °C for 12 h. The order-disorder transition temperature was identified by small-angle x-ray scattering (SAXS) at ~230 °C. The χN at 50 °C is estimated to be 24.7 [16], suggesting that the sample is in the weak segregation regime. The microphase-separated sample was then subjected to a large-amplitude planar shear at 120 °C under a dry argon atmosphere, using a laboratory-built shear apparatus. The shear frequency was 0.5 Hz, and the amplitude was 150%. The shear direction is defined as the *x* direction, and the shear gradient is along the *z* direction. After shear, the sample was quenched to room temperature. A small piece

of the sample ($\sim 1.0 \times 1.0 \times 0.2$ mm^3) was used for SAXS study.

Two-dimensional (2D) SAXS experiments were performed at the synchrotron x-ray beam line X27C of the National Synchrotron Light Source in Brookhaven National Laboratory using imaging plates as detectors. The x-ray wavelength was $\lambda = 0.1307$ nm, and the scattering vector ($q = 4\pi \sin\theta/\lambda$, where 2θ is the scattering angle) was calibrated with silver behenate. Transmission electron microscopy (TEM) experiments were carried out on a JEOL 1200 EX II at 120 kV. Thin sections for TEM were obtained using a Reichert Ultracut S (Leica) microtome at −40 °C. Samples were subsequently stained using RuO$_4$ vapor at room temperature for 20 min [17].

The 2D SAXS patterns along the *x*, *y*, and *z* directions are shown in Figs. 1a–1c, respectively. The sharp SAXS reflections are caused by the PEO crystallization [16]. Besides the primitive unit cell, the $R\bar{3}m$ structure can also be presented using a nonprimitive hexagonal cell. Therefore, we use hexagonal indices (*hkil*) to index both the trigonal and hexagonal reciprocal lattices. Careful inspection of the x-ray patterns reveals that the patterns comprised two superposed structures: trigonal *ABCABC* ($R\bar{3}m$) and hexagonal *ABAB* ($P6_3/mmc$) stackings. The calculated SAXS patterns are shown in Figs. 2a–2c. In order to fit the experimental observation in Fig. 1a with the calculated SAXS pattern along the $[\bar{1}2\bar{1}0]$ (the *x*) direction in Fig. 2a, we need to superpose equally twinned trigonal reciprocal lattices with a hexagonal reciprocal lattice. Note that the trigonal twins have sequences of *ABCABC* and *ACBACB*, respectively. It is recognized in the mixed pattern of Fig. 2a that in every third layer the reciprocal lattices of the two trigonal components overlap to form a *partial merohedral* twinning and the twin element is the {0003} plane. In Fig. 2b, the trigonal twins give an identical diffraction pattern along the $[10\bar{1}0]$ (the *y*) direction, and this pattern is superposed with the hexagonal diffraction pattern to construct a mixed pattern as shown in
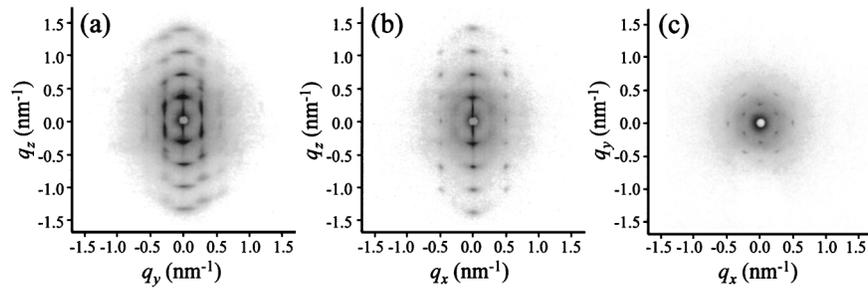
FIG. 1.   High-resolution synchrotron SAXS patterns along the x (a), y (b), and z (c) directions.

Fig. 2b. This mixed pattern provides good correspondence with the experimental observation along the y direction of Fig. 1b. The $[000l]$ SAXS pattern along the z direction provides direct evidence for the existence of the hexagonal structure. The trigonal twins again show identical diffractions in the z direction. However, the first order reflections of the trigonal reciprocal lattice are extinct for $R\bar{3}m$ [18]. Therefore, the sixfold first order reflections must solely
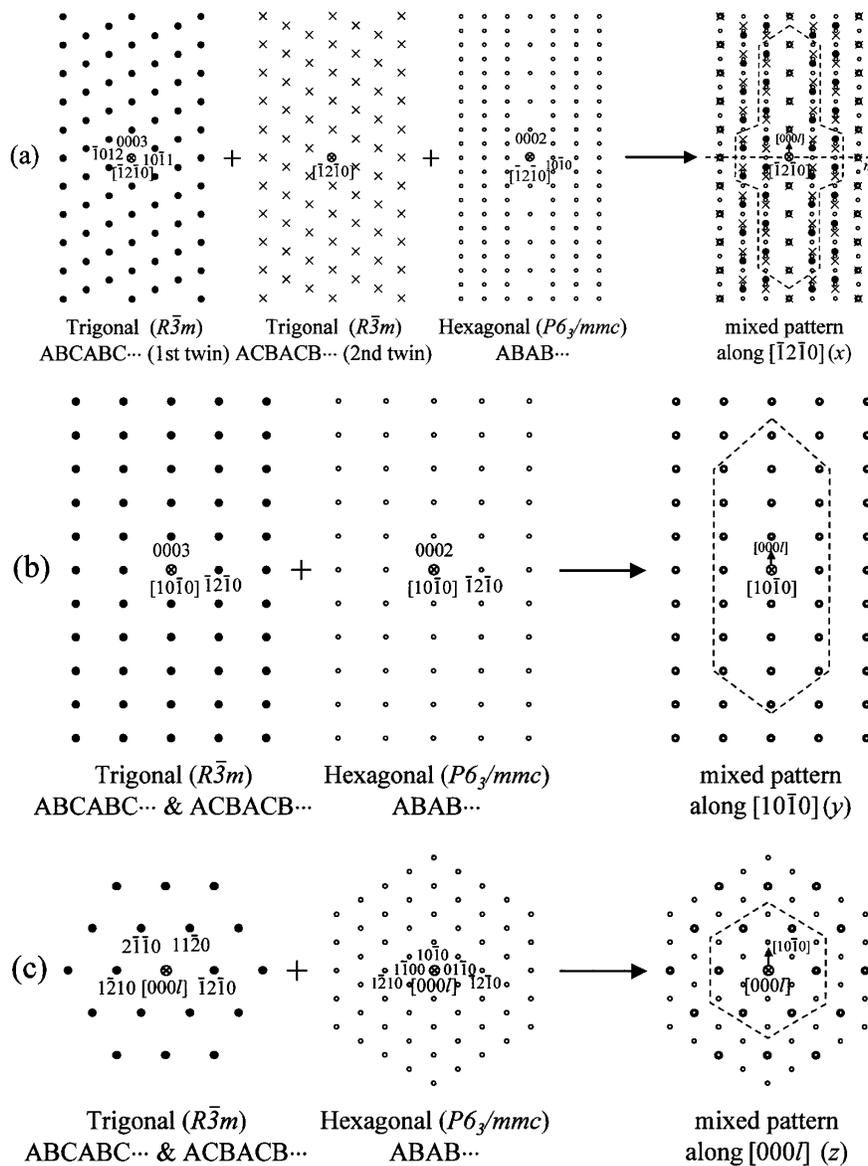

FIG. 2.   X-ray crystallographic analyses for the SAXS patterns along the $[\bar{1}2\bar{1}0]$ (a), $[10\bar{1}0]$ (b), and $[000l]$ (c) directions. Note that both trigonal and hexagonal structures use hexagonal lattice indices.

result from a hexagonal lattice, which has the same a and α values but a different c dimension. Thus, the mixed pattern along the z direction in Fig. 2c also fits our experimental observation in Fig. 1c.

From the above x-ray crystallographic analyses the primitive unit-cell parameters for the trigonal lattice are determined to be $a_t = b_t = c_t = 24.3$ nm and $\alpha_t = \beta_t = \gamma_t = 66.3°$, and the hexagonal lattice has unit-cell parameters of $a_h = 26.6$ nm, $c_h = 37.8$ nm, and $\alpha_h = 120°$. If the nonprimitive hexagonal cell is used to describe the trigonal cell, the new unit cell possesses identical a and α values as the hexagonal cell, but the c axis becomes $c_h^t = 3c_h/2 = 56.7$ nm. Therefore, one layer thickness in the HPL phase is $d = c_h/2 = c_h^t/3 = 18.9$ nm. Moreover, judging from the intensity difference between the $10\bar{1}0$ reflections in the hexagonal lattice and the $10\bar{1}1$ reflections in the trigonal lattice in Fig. 1a (note that both are first order reflections), one can qualitatively estimate that the population of the hexagonal phase is less than that of the trigonal twins, although the structure factors for both structures are unavailable.

It is interesting that both the trigonal and hexagonal structures in the HPL phase have identical in-plane bond and orientational orders. These two phases must be interrelated and we speculate that they are induced by plastic deformation during mechanical shear (similar to mechanical slip in metals [19]). In order to visualize the plastic deformation in real space, a TEM study was carried out to understand the interrelationship between these two structures. It should be noted that the trigonal and hexagonal structures in the HPL phase can be easily differentiated through a 2D TEM projection image along the $[\bar{1}2\bar{1}0]$ (the x) direction.

Bright-field TEM micrographs of RuO_4 stained thin sections have been taken, and Fig. 3a is one example. The alternating perforated layers ($\{0003\}$ planes) are oriented in the horizontal direction. Since the PEO phase is more easily stained than the PS phase [16], the PEO phase pro-

jections are darker than those of the PS phases in Fig. 3a. To clarify our analysis, a reproduction of the 2D TEM pattern is shown in Fig. 3b. At the top left part of Fig. 3b a trigonal $ABCABC$ stacking can be identified, while the hexagonal $ABAB$ stacking is observed in the bottom left. Different edge dislocations can be recognized in this micrograph. The first type is the *Frank partial dislocation* (see ⊣ or ⊢ label in Fig. 3b). A Frank dislocation loop can be formed by the absence of a layer ("vacancy loop") with the subsequent collapsing of the surrounding layers. Therefore, the Burgers vector of the Frank partial dislocations is $\mathbf{b}_F = c/3\langle 0003 \rangle$. For the "vacancy loop," by removing a layer, e.g., a B layer at ⊣$_1$ in Fig. 3b, the stacking sequence changes from the original $ABCABCA$ to $ABCA\!\!\downarrow\!\!CA$ sequence (area I in Fig. 3b), where the vertical arrow indicates the position of an intrinsic stacking fault. Note that this fault creates a four-layer hexagonal $CACA$ sequence. By inserting a C layer at ⊢ in Fig. 3b ("interstitial loop"), the normal $ABCABC$ sequence becomes an $ABCA\!\!\downarrow\!\!\downarrow\!\!C\!BC$ sequence (area II in Fig. 3b), which represents an extrinsic stacking fault.

A second type of edge dislocation evident in the image is the *unit (perfect) dislocation* (see ⊥ or ⊤ label in Fig. 3b). These defects correspond to $\{0003\}\langle\bar{1}2\bar{1}0\rangle$ slip. It has a Burgers vector, $\mathbf{b}_U = a\langle\bar{1}2\bar{1}0\rangle$, and is always dissociated into two *Shockley partial dislocations.* Each Shockley partial dislocation has a Burgers vector, $\mathbf{b}_S = a/3\langle 10\bar{1}0\rangle$. In principal, the relative energies involved in the Shockley partial dislocation (E_S), Frank partial dislocation (E_F), and unit dislocation (E_U) have a relationship of $E_S : E_F : E_U = 1 : 2 : 3$. Therefore, Shockley partial dislocations are the most frequent defects under plastic deformation. In general, a single $a/3\langle 10\bar{1}0\rangle$ shear produces an intrinsic stacking fault, while a second shear on the adjacent plane causes an extrinsic stacking fault. Both these stacking defaults are geometrically equivalent to those formed by the Frank partial dislocation. If Shockley partial dislocations
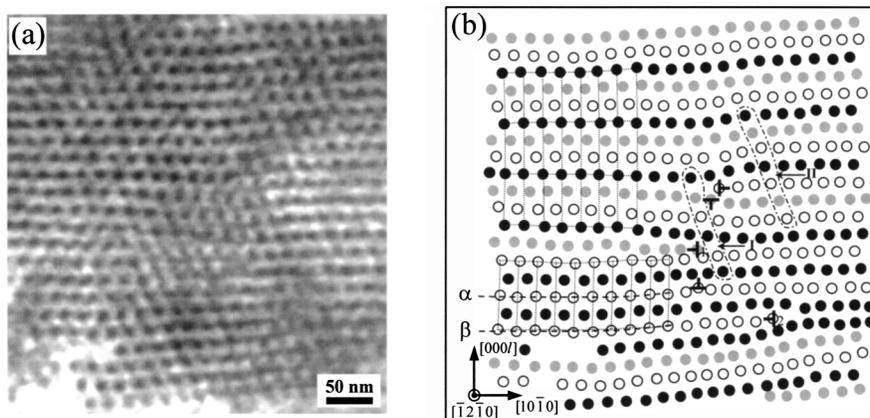

FIG. 3. (a) Bright-field TEM image of a RuO_4 stained thin slice PEO-b-PS sample sectioned perpendicular to the x direction. (b) A schematic reproduction of the TEM 2D lattice. The dark, gray, and white symbols represent the PEO domains in the A, B, and C layers, respectively. The stacking sequence is labeled based on the lattice analysis.

occur successively on the second layer from a previous dislocation line, a relatively large hexagonal domain can be formed. There are two intrinsic stacking faults in the bottom left part of Fig. 3b where two Shockley dislocation lines, α and β, are evident. The β is formed by a next Shockley partial dislocation on the second layer from the α.

If the $a/3\langle 10\bar{1}0\rangle$ shear is carried out plane by plane above an A layer (i.e., a series of intrinsic stacking faults on neighboring planes), a coherent twin is produced (e.g., $ABCA\overset{\downarrow}{C}B\overset{\downarrow}{A}\overset{\downarrow}{C}B$). This explains our analysis of the SAXS pattern along the x direction (Figs. 1a and 2a). It is speculated that the {0003} twinning in the HPL phase may be polysynthetic (lamellar) twins with relative large grain sizes, similar to those in minerals and metals [20]. Note that deformation twinning is energetically more favorable, since the stacking-fault energies for twin (γ_{twin}), intrinsic (γ_{int}), and extrinsic (γ_{ext}) stacking faults usually possess a relationship of $2\gamma_{\mathrm{twin}} \approx \gamma_{\mathrm{int}} < \gamma_{\mathrm{ext}} < 2\gamma_{\mathrm{int}}$. Therefore, the trigonal twin structures should be a major component under plastic deformation, as observed in our SAXS results.

In summary, the plastic deformation-induced HPL phase is identified as a mixture of majority trigonal ($R\bar{3}m$) twins and minority hexagonal ($P6_3/mmc$) structure. The hexagonal structure is generated by either Shockley or Frank partial dislocations through sequential intrinsic stacking faults on the second layer from a previous dislocation line, and the trigonal twin structures are formed by successive intrinsic stacking faults on neighboring layers due to plastic deformation. We thus conclude that the HPL phase is controlled by dislocations under mechanical shear, and none of the trigonal twins or hexagonal structure is in equilibrium.

---

*To whom correspondence should be addressed.
Email address: cheng@polymer.uakron.edu

[1] F. S. Bates and G. H. Fredrickson, Annu. Rev. Phys. Chem. **41**, 525 (1990).
[2] D. A. Hajduk, P. E. Harper, S. M. Gruner, C. C. Kim, E. L. Thomas, and L. J. Fetters, Macromolecules **27**, 4063 (1994).
[3] M. F. Schulz, F. S. Bates, K. Almdal, and K. Mortensen, Phys. Rev. Lett. **73**, 86 (1994).
[4] E. L. Thomas, D. M. Anderson, C. S. Henkee, and D. Hoffman, Nature (London) **334**, 598 (1988).
[5] R. J. Spontak, S. D. Smith, and A. Ashraf, Macromolecules **26**, 956 (1993).
[6] M. M. Disko, K. S. Liang, S. K. Behal, R. J. Roe, and K. J. Jeon, Macromolecules **26**, 2983 (1993).
[7] K. Almdal, K. A. Koppi, F. S. Bates, and K. Mortensen, Macromolecules **25**, 1743 (1992).
[8] I. W. Hamley, K. A. Koppi, J. H. Rosedale, F. S. Bates, K. Almdal, and K. Mortensen, Macromolecules **26**, 5959 (1993).
[9] S. Förster, A. K. Khandpur, J. Zhao, F. S. Bates, I. W. Hamley, A. Ryan, and W. Bras, Macromolecules **27**, 6922 (1994).
[10] M. E. Vigild, K. Almdal, K. Mortensen, I. W. Hamley, J. P. A. Fairclough, and A. J. Ryan, Macromolecules **31**, 5702 (1998).
[11] J. H. Ahn and W. C. Zin, Macromolecules **33**, 641 (2000).
[12] M. Laradji, A. C. Shi, R. C. Desai, and J. Noolandi, Phys. Rev. Lett. **78**, 2577 (1997).
[13] S. Qi and Z. G. Wang, Macromolecules **30**, 4491 (1997).
[14] P. D. Olmsted and S. T. Milner, Macromolecules **31**, 4011 (1998).
[15] D. A. Hajduk, H. Takenouchi, M. A. Hillmyer, F. S. Bates, M. E. Vigild, and K. Almdal, Macromolecules **30**, 3788 (1997).
[16] L. Zhu, S. Z. D. Cheng, B. H. Calhoun, Q. Ge, R. P. Quirk, E. L. Thomas, B. S. Hsiao, F. Yeh, and B. Lotz, Polymer **42**, 5847 (2001).
[17] J. S. Trent, J. I. Scheinbeim, and P. R. Couchman, Macromolecules **16**, 589 (1983).
[18] *International Tables for Crystallography,* edited by T. Hahn (Kluwer Academic Publishers, Dordrecht, 1996).
[19] W. Hume-Rothery, R. E. Smallman, and C. W. Haworth, *The Structure of Metals and Alloys* (The Institute of Metals, London, 1988).
[20] *Deformation Twinning,* edited by R. E. Reed-Hill, J. P. Hirth, and H. C. Rogers (Gordon and Breach, New York, 1964).